Nano Energy (2015) 13, 346–354

Available online at www.sciencedirect.com

ScienceDirect

journal homepage: www.elsevier.com/locate/nanoenergy

RAPID COMMUNICATION

Nanocellulose as green dispersant for two-dimensional energy materials

Yuanyuan Li[a,b,1], Hongli Zhu[a,1], Fei Shen[a], Jiayu Wan[a], Steven Lacey[a], Zhiqiang Fang[a], Hongqi Dai[b,*], Liangbing Hu[a,*]

[a]*Department of Materials Science and Engineering, University of Maryland, College Park, MD 20742 USA*
[b]*College of Light Industry Science and Engineering, Nanjing Forestry University, Nanjing, Jiangsu 210037, PR China*

Received 10 December 2014; received in revised form 9 February 2015; accepted 11 February 2015
Available online 21 February 2015

KEYWORDS
Nanofibrillated cellulose;
Dispersant;
Two-dimensional material;
Films/fibers;
Sodium ion battery

Abstract
The exfoliation/dispersion of two-dimensional (2D) materials is of great importance due to their unique properties and applications in electronics as well as energy storage devices. In this paper, we address the challenge of dispersing 2D materials in a scalable and environmentally friendly way. A methodology to efficiently disperse 2D materials [boron nitride (BN) and molybdenum disulfide (MoS_2)] in an aqueous solution using a green dispersant, nanofibrillated cellulose (NFC), was introduced. The stable high concentration BN/MoS_2 aqueous solutions allow the formation of multifunctional composites and may facilitate roll-to-roll manufacturing. Films and fibers with excellent mechanical strength were fabricated with the BN solution. Additionally, strong and flexible MoS_2 films were prepared and used as anodes for sodium ion batteries, indicating flexible battery applications.

Introduction

Two-dimensional (2D) materials with strong in-plane bonds but weak out-of-plane bonds have been extremely popular in research endeavors since the discovery of monolayer graphene in 2004 [1]. Besides graphene, there are numerous 2D materials such as boron nitride (BN), transition metal dichalcogenides (MoS_2, WS_2), and transition metal oxides (MoO_3, MnO_2) that exhibit interesting properties and offer a wide range of applications from electronics to the life sciences [2–4]. For instance, BN is an electronically insulating material with excellent thermal conductivity and stability. These unique properties make BN an outstanding candidate for many applications that are not possible for graphene [5,6]. Molybdenum disulfide (MoS_2) has also garnered much attention in electronics and as a photovoltaic

*Corresponding authors.
E-mail addresses: daihq@njfu.com.cn (H. Dai), binghu@umd.edu (L. Hu).
[1]These authors contributed equally to this work.

http://dx.doi.org/10.1016/j.nanoen.2015.02.015
2211-2855/

material due to its strong absorption in the solar spectral range [7].

The exfoliation/dispersion of 2D materials yields materials with a very high surface area which is attractive in surface active and catalytic materials. The electronic band structure can also be modified through exfoliation/dispersion since the electrons are constrained to adopt a 2D wave function after exfoliation/dispersion [8,9]. For example, the band gap of bulk MoS_2 (indirect) and dispersed monolayer flakes (direct) differ dramatically. The changes in the electronic structure cause the monolayer flakes to exhibit strong photoluminescence [10,11]. The proper exfoliation method is essential to obtain a large quantity of high quality flakes. Numerous methods have been developed to disperse 2D materials; however, liquid exfoliation/dispersion remains superior since the process is potentially scalable, can lead to roll-to-roll manufacturing, and the obtained ink allows for the formation of multifunctional composites [12]. A dispersion method that utilizes greener solvents and dispersants can enable cost-effective large-scale production processes that minimize or eliminate the need for properly disposing potentially harmful chemicals [13-15].

Nanocellulose, mainly derived from wood with diameters in the nanoscale and lengths in the microscale, is considered to be a low-cost, green and inexhaustible material [16]. Owing to its impressive optical, mechanical, and thermal properties, nanocellulose has been extensively studied as a building block for films and fibers, a separator for batteries, and a substrate for electronic devices [17-21]. The presence of polar –OH groups enables hydrophilicity while the exposure of hydrophobic –CH moieties causes hydrophobic faces to form in the elementary fibrils. The existence of both hydrophilic and hydrophobic faces allows cellulose to be used as a dispersant [22]. Previously, nanocellulose has been reported as an emulsifier for perking emulsions [23], a stabilizer for magnetic nanoparticles [18] as well as a dispersant for carbon nanotubes (CNTs) [24]. The use of nanocellulose to disperse 2D energy materials is a novel concept that should be explored.

In this paper, 2,2,6,6-tetramethylpiperidine-1-oxyl (TEMPO)-oxidized nanofibrillated cellulose (NFC) was used as a dispersant to disperse 2D materials (BN and MoS_2) in water. Fig. 1 illustrates the mechanism for the dispersion of 2D materials by NFC: NFC attaches to the flakes through the interaction between its hydrophobic sites and the flake's hydrophobic plane as well as hydrogen bonding between the NFC hydroxyl groups and the defective edges of the 2D materials. The flakes are stabilized due to steric hindrance and the electrostatic repulsive forces generated by the charged NFC carboxyl groups. This method is more suitable for green, large-scale dispersion of 2D materials since proper disposal of the solvent is a non-issue. Composite films were fabricated using the NFC-assisted dispersed BN and MoS_2 aqueous solutions with great mechanical strength: 182 ± 16 MPa and 159 ± 18 MPa respectively. These values are among the highest achieved for composites with identical 2D material content [12,25-29]. Sodium ion batteries were also assembled with the MoS_2 films acting as an anode, indicating flexible battery applications.

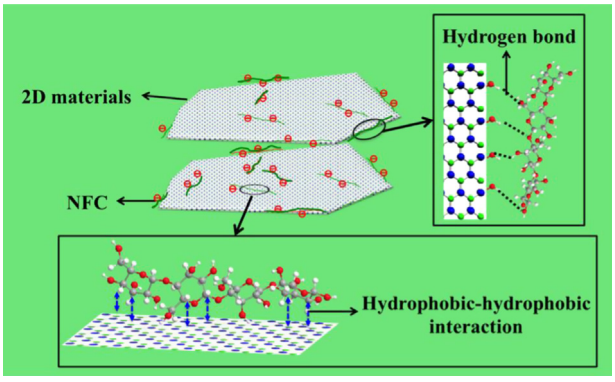

Fig. 1 Schematic to show how NFC disperses 2D materials. C, O, and H atoms are represented as gray, red, and white spheres, respectively. ⊖ represents the negative surface charge introduced by NFC carboxyl groups. (For interpretation of the references to color in this figure legend, the reader is referred to the web version of this article.)

Experimental

NFC preparation

NFC was prepared according to a previously reported method [30]. Briefly, TEMPO (78 mg), sodium bromide (NaBr, 514 mg) and Kraft bleached softwood pulp (5 g) were mixed together. Then 10 mmol sodium hypochlorite (NaClO) was added under gentle agitation at room temperature to trigger the TEMPO oxidation of the cellulose fibers. During the oxidation process, the pH was maintained at 10.5 by adding sodium hydroxide (NaOH). The reaction ended when all the NaClO was consumed. After TEMPO treatment, the fibers were thoroughly washed with distilled water and disintegrated by one pass through a Microfluidizer M-110EH (Microfluidics Ind., USA) to obtain an NFC suspension. To evaluate the dispersion's stability, the Zeta potential was determined using a Zetasizer Nano ZS90 equipment. The concentration of the NFC solution for the Zeta potential tests was 0.3 wt% at a pH of 7.7 (Malvern Instruments, Worcestershire, UK). Atomic force microscopy (AFM) (Dimension FastScan, Bruker Corporation) was applied to characterize the morphology of NFC in tapping mode.

BN and MoS_2 dispersion

Commercial BN powder (Graphene Supermarket Inc., average particle size of 5 μm) and 10 wt% NFC (relative to BN powder) were mixed together in water with an initial BN concentration of 5 mg/mL. The exfoliation/dispersion process was performed through bath sonication for 30 h (FS 110D, Fisher Scientific). After sonication, the dispersion was then centrifuged at 3000 rpm for 15 min and the supernatant was kept. The absorbance spectrum of the BN dispersion was obtained with a UV-vis Spectrometer Lambda 35 (PerkinElmer, USA). The Zeta potential was determined using the Zetasizer Nano ZS90 equipment with a BN dispersion concentration of 0.7 mg/mL and a pH value of 7.8. (Malvern Instruments, Worcestershire, UK). The morphology of dispersed BN flakes was characterized by transmission electron microscopy (TEM) using a JEOL JEM 2100 (Japan) at an accelerating voltage of 200 kV.

MoS_2 was exfoliated with two different NFC additions: 10 wt% and 50 wt% NFC (relative to the MoS_2 mineral). Commercial MoS_2 mineral (SPI Supplies) and its respective NFC addition were mixed together in water with a mineral concentration of 5 mg/mL. The exfoliation/dispersion was performed through bath sonication for 4 h (FS 110D, Fisher Scientific) before being centrifuged at 5000 rpm for 15 min. After centrifugation, the supernatant was kept and acted as the dispersion. The absorbance spectrum of the MoS_2 dispersion was obtained with a UV–vis Spectrometer Lambda 35 (PerkInElmer, USA). The Zeta potential was tested using the Zetasizer Nano ZS90 equipment with a MoS_2 dispersion concentration of 0.3 mg/mL at a pH of 7.8. (Malvern Instruments, Worcestershire, UK). The morphology of dispersed MoS_2 flakes was characterized by transmission electron microscopy (TEM) using a JEOL JEM 2100 (Japan) at an accelerating voltage of 200 kV.

Film/fiber fabrication and characterization

BN and MoS_2 films were fabricated by filtering the previously prepared dispersions. The obtained wet films were dried at room temperature under pressure. Films with different NFC content were made from BN–NFC (4 wt% BN, 40 wt% BN, 75 wt% BN) and MoS_2–NFC (13 wt% MoS_2, 25 wt% MoS_2) hybrid solutions. The hybrid solutions were prepared by adding NFC into BN and MoS_2 dispersions before sonicating the solutions for 1 min. BN fibers were fabricated by wet spinning. To be specific, a NFC-assisted dispersed BN solution (17 mg/mL) was extruded directly into ethanol through a springe. A gel fiber was formed in ethanol and pulled out to dry in air after 1 min of immersion. A force was applied at the ends of the fibers by hand to dry them under tension. The morphology and thickness of the films and fibers were characterized with a Hitachi SU-70 field emission scanning electron microscope (FESEM) and optical microscope. The tensile strength was determined using a dynamic mechanical analysis (DMA) machine (Q800) in tension film mode. Before testing, each sample was conditioned for 24 h at 50% humidity under a temperature of ~23 °C. Each film was cut into a strip (3 mm × 20 mm) for testing.

Battery assembling and testing

The conductive MoS_2 film was fabricated by filtering an NFC dispersed MoS_2 solution mixed with CNTs and drying it in a vacuum oven at 100 °C. The weight ratio of MoS_2:NFC:CNT was 67:16.5:16.5. Half-cells were assembled using 3/8″ MoS_2 films as the working electrode and sodium metal (99%, Sigma-Aldrich) as the counter electrode. The separator and 2025 coin cell were purchased from MTI Inc. 1 M $NaPF_6$ in ethylene carbonate (EC)-dimethyl carbonate (DMC) served as the electrolyte. MoS_2 cells with NFC-free dispersed MoS_2 films as working electrode were made in the same process as control samples, while the weight ratio of MoS_2:CNT was 83.5:16.5. The assembled cells were tested using a Biologic VMP3 electrochemical potentiostat in the potential range of 0.1–2.35 V at 10 mA/g.

Results and discussion

Nanocellulose is one of the most inexhaustible renewable polymers. It is considered to be amphiphilic due to the presence of both polar –OH groups and non-polar –CH moieties [22]. In this work, NFC was applied to disperse 2D materials such as BN and MoS_2. TEMPO-oxidized cellulose fibers were passed through a microfludizer to create NFC with a length and diameter of approximately 200–500 nm and 10–20 nm respectively (Fig. 2a). The obtained NFC solution was transparent as shown in Fig. S1a. NFC was stable in water due to the introduction of charged carboxyl groups. The Zeta potential of the NFC solution was −64.9 mV, indicative of a highly stable solution. 2D materials such as BN (Fig. S1b) and MoS_2 (Fig. S1c) were chosen due to their unique thermal and electronic properties as well as the challenge to disperse them efficiently.

With the addition of NFC, dispersed BN solution with a concentration up to 1.1 mg/mL was obtained (details about calculating the BN concentration is in Supporting information). The dispersion yield (the weight ratio of exfoliated BN to bulk BN) reached 22%, which is among the highest yield reported for BN by sonication [31]. Note that NFC-assisted dispersed BN solution demonstrated better stability compared to the BN dispersion without NFC as shown in Fig. 2b. After sitting for 10 days, clear aggregates appeared in the BN dispersion without NFC while NFC-assisted dispersed BN solution remained stable. The same phenomenon was observed for the MoS_2 dispersions as well. Without the addition of NFC, the dispersed MoS_2 solution was not stable and began to precipitate after sitting for 1 day. However, NFC-assisted dispersed MoS_2 solutions were stable even after 2 months (Fig. 2c). It is likely that the electrostatic repulsion between the charged carboxyl groups on the NFC helps to stabilize the flakes. The Zeta potential of the NFC-assisted dispersed BN and MoS_2 solutions were −41.9 mV and −38.3 mV respectively, which demonstrates the solution's stability and supports the proposed stabilizing mechanism *via* electrostatic repulsion. Beyond electrostatic repulsive forces, May et al. demonstrated that a steric stabilization mechanism was also attributed to the polymer stabilized 2D flakes [32]. Thus, the stabilization of NFC-assisted dispersed 2D flakes likely corresponds to both electrostatic repulsion and steric hindrance.

With the help of NFC, the exfoliation/dispersion yield of MoS_2 can reach 18%. The solution without NFC displayed a lighter color than the NFC-assisted dispersed solution. This indicates that the addition of NFC enables a superior dispersion of MoS_2 (Fig. 2c). Note that the concentration of the MoS_2 solution with 10 wt% NFC was 0.3 mg/mL while 50 wt% NFC was 0.9 mg/mL. Based on these concentrations, the higher NFC addition clearly enhanced the dispersion of MoS_2 in the water solutions (Fig. 2c and Fig. S1d). The entire NFC-assisted MoS_2 dispersion process took 4 h. This process is much more efficient than dispersion by ion-intercalation which requires more than 20 h to complete [33]. Note that NFC can disperse BN and MoS_2 efficiently with only 10 wt%, which is a much lower dosage than dispersions reported in polymer solutions [32]. The NFC addition is even lower than a surfactant-assisted dispersion which requires 30 wt% of 2D materials [34]. Additionally, this NFC-assisted dispersion method is scalable since approximately 200 mL of exfoliated

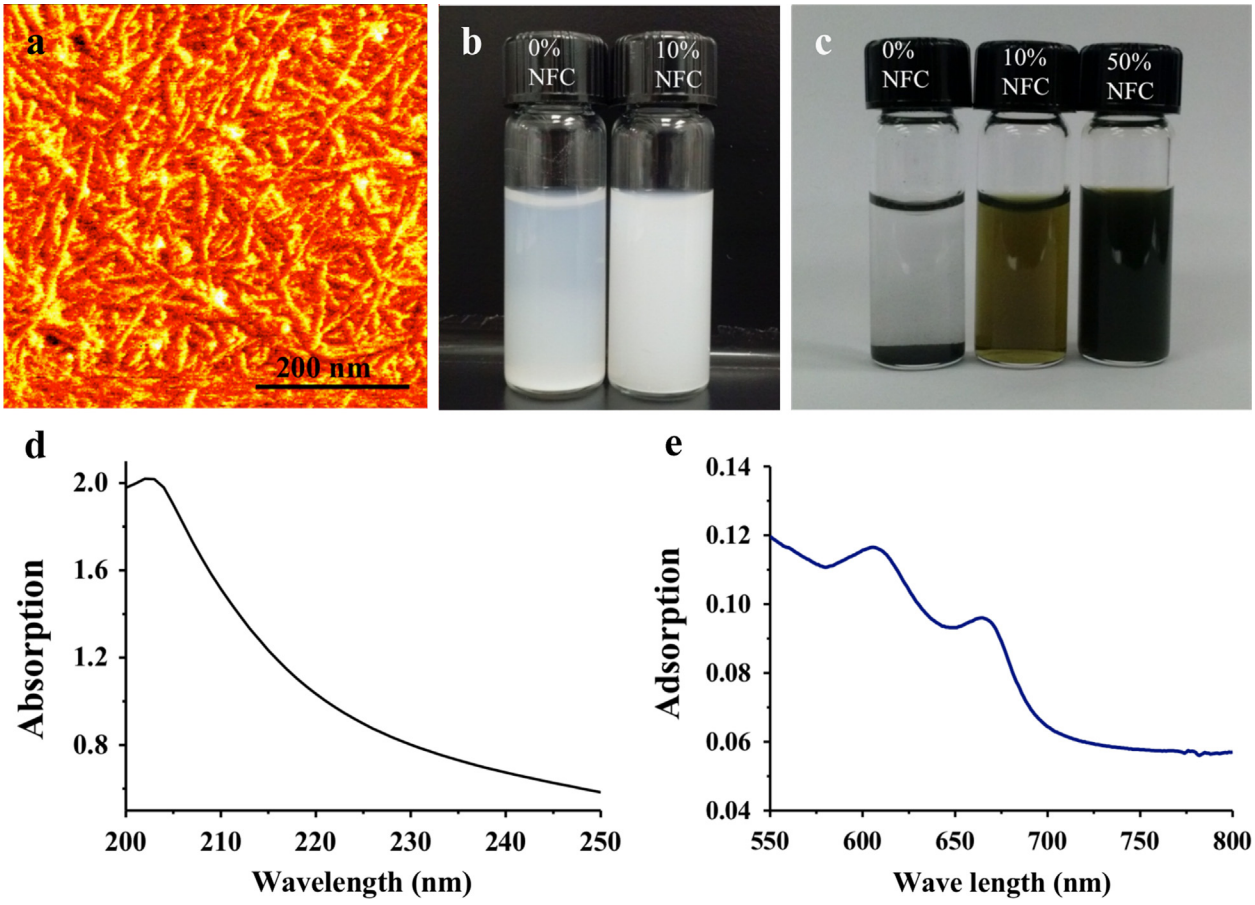

Fig. 2 (a) An AFM image of NFC. (b) A digital image of exfoliated/dispersed BN in water without NFC and with 10% NFC after sitting for 10 days after centrifugation. (c) MoS_2 dispersions with different NFC content after centrifugation and sitting for 2 months. (d and e) UV-vis absorption spectra of BN and MoS_2 water solutions respectively.

2D material dispersions can be easily obtained at once (Fig. S1e and f).

To confirm the result of well-dispersed 2D flakes, the solutions were characterized using UV-vis absorbance spectroscopy. Fig. 2d is the absorption spectrum of the BN dispersion. The spectrum exhibits a peak at 203 nm, which is in agreement with the wavelength of reported exfoliated BN dispersions [35]. Fig. 2e shows the typical absorption spectrum for a MoS_2 water solution with two peaks centered at 605 nm and 664 nm. These peaks are consistent with the MoS_2 flakes obtained by grinding-assisted liquid phase exfoliation [36]. In conclusion, these results exhibit well-dispersed monolayer or few-layer nanosheets in the solvent mixtures.

Transmission electron microscopy (TEM) was utilized to characterize the size of the dispersed flakes. The lateral size of the BN flakes was 50–300 nm for the dispersion without NFC (Fig. 3a). The NFC-assisted dispersed flakes were larger with a lateral size ranging from 200 nm to micrometers (Fig. 3b and c). For the MoS_2 flakes, the lateral size of the dispersed flakes with and without NFC ranged from 200 nm to micrometers and 50 nm to 500 nm respectively (Fig. 3d-f). This difference may be due to poor stress transfer during the cavitation process at the water/NFC/2D material interface [37]. In order to provide evidence of NFC's tendency to attach to flakes, elemental mapping was conducted on the NFC dispersed BN flakes. Fig. 3g is the original TEM image used to take these elemental maps. The N and B elemental maps shown in Fig. 3h and i demonstrated that the flake is truly BN. Fig. 3j shows the elemental map for O, indicative of NFC attached to the BN flake.

NFC has been shown to be an effective dispersant for BN and MoS_2 flakes in water. To understand the NFC-assisted dispersing mechanism of BN and MoS_2, the surface properties of NFC need to be investigated. NFC is believed to be hydrophilic due to the polar hydroxyl groups; however, hydrophobic faces also exist due to the exposure of hydrophobic –CH moieties (Fig. 4a and b) [38]. Although the hydrophobic surfaces are less representative, cellulose still possesses the property to capture nonpolar solvents such as chloroform or cyclohexane and interact with the hydrophobic aromatic moieties of lignin and the hydrophobic cellulose-binding modules of cellulases [39]. In order to verify NFC's amphiphilic properties, NFC was added into an 80% water/20% oil (hexane) mixture. A water-oil emulsion formed after sonicating for 10 min (Fig. 4c), which verifies that NFC has an affinity to both water and oil. This helped to prove the potential of NFC to attach to hydrophobic 2D flakes through the interaction between the NFC hydrophobic surfaces and the 2D flakes. For the dispersion of BN and MoS_2 flakes, we believe this may pertain to two kinds of interactions between the NFC and the 2D flakes: hydrophobic to hydrophobic interactions as well as hydrogen bonding. Previous studies have shown that both BN and MoS_2 flakes contained hydroxyl

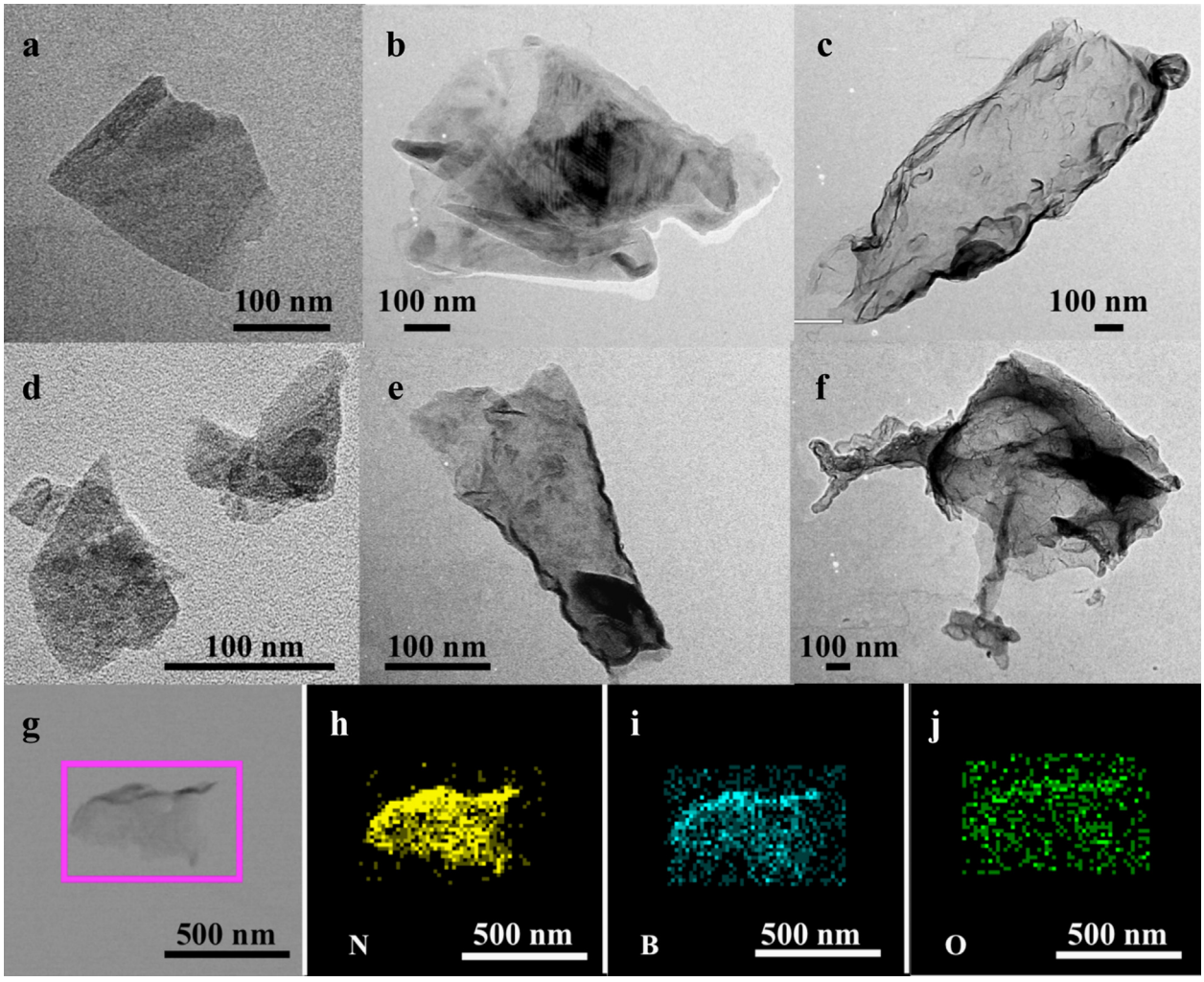

Fig. 3 TEM images of BN dispersed in water (a) without NFC and (b and c) with NFC. TEM images of MoS_2 dispersed in water (d) without NFC and (e and f) with NFC. (g–j) Elemental mapping of a BN flake to show the presence of cellulose: (g) TEM image and the elemental mapping of (h) N, (i) B, and (j) O.

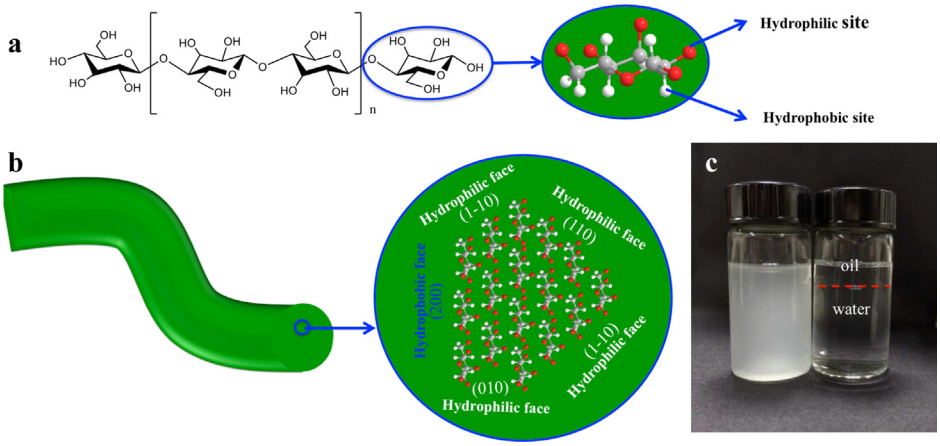

Fig. 4 (a) Chemical structure of cellulose where a 3D structure of glucose shows the hydrophilic and hydrophobic sites. (b) Schematic of a cellulose crystal in an elementary fibril with hydrophobic and hydrophilic faces [38], among them, the (200) face refers to the hydrophobic face while the (1 − 10), (110), (1 − 10), (010) refer to hydrophilic faces. C, O, and H atoms are represented as gray, red, and white spheres, respectively. Note that only major components of hydrogen bonds are represented. (c) Image of a water–oil emulsion with the presence of NFC (left) and water–oil mixture before the addition of NFC (right). (For interpretation of the references to color in this figure legend, the reader is referred to the web version of this article.)

groups after sonication-assisted hydrolysis in water [35,40,41]. This causes the flakes to exhibit an affinity with NFC through hydrogen bonding. Charges are introduced to the 2D flakes due to the attachment of NFC. The electrostatic repulsive forces of the charged NFC carboxyl groups attached to BN/MoS_2 flakes as well as the steric hindrance formed by the NFC prevents the dispersed flakes to re-aggregate. This leads to the formation of stable dispersions.

Based on the obtained dispersions, films with thicknesses in the nanoscale and microscale can be fabricated *via* methods such as spray coating, filtration, and casting. Through filtration of the NFC-assisted dispersed BN solution, flexible BN composite films can be obtained and folded into an origami crane (Fig. 5a). Note that the layered structure of the BN film is evident in the cross-sectional SEM images shown in Fig. 5b and Fig. S2a. The layers formed by the NFC and BN flakes can act as multi-walls to protect materials against oxygen, which is important for specific applications [20]. Fig. S2b is the surface SEM image of the BN composite film, which depicts how NFC glues the BN flakes together. The BN film fabricated using the NFC dispersed BN solution also possessed great mechanical strength. Fig. 5c shows the typical stress-strain curve of the BN film containing 40 wt% BN. BN-NFC nanocomposites with 75 wt%, 40 wt%, and 4 wt% of BN exhibited a tensile strength of 80 ± 4 MPa, 100 ± 5 MPa, and 182 ± 16 MPa respectively. These values are higher than other BN nanocomposites at the same BN content as depicted in Fig. 5d. The excellent mechanical strength was ascribed to the presence of NFC which acts as both a strong building block and as a strengthening agent to connect the BN flakes together [19]. Additionally, the one-dimensional fibers with 2D plates act as a structural analog to what researchers typically use to create strong films: a nacre (comprised of well-ordered, layered plates with a polymer coating) [42]. The resulting film shows superior thermal conductivity and mechanical strength. For the 50 wt% BN hybrid film, a high thermal conductivity comparable to aluminum alloys can be obtained with values up to 145.7 W/m K [4]. This BN hybrid films have great potential applications in electronic devices based on their thermally conductive and electrically insulating properties.

It is difficult to make stable BN-polymer solutions with more than 10 wt% BN dispersed in an organic solvent due to the poor compatibility of the organic solvent with water. Our NFC-assisted dispersed BN water solutions avoided this problem by forming a gel after the water evaporation. Fig. S2c shows the NFC exfoliated BN gel with a concentration of 17 mg/mL. By extruding the gel into ethanol through a springe, BN fibers were produced as shown in Fig. 5e and Fig. S2d. Fig. 5e is the polarized optical microscopy (POM) image of the BN fiber obtained when the fiber is rotated to an angle of 45° with respect to the polarizer. This demonstrates the high level of alignment of the building block along the fiber. The BN fiber containing 40 wt% BN exhibited a tensile strength of 244 ± 4 MPa (Fig. 5f). Note that the mechanical strength of the fiber was higher than the film under the same BN loading. This was mainly due to increased alignment of the building blocks within the fiber. The fibers were not only

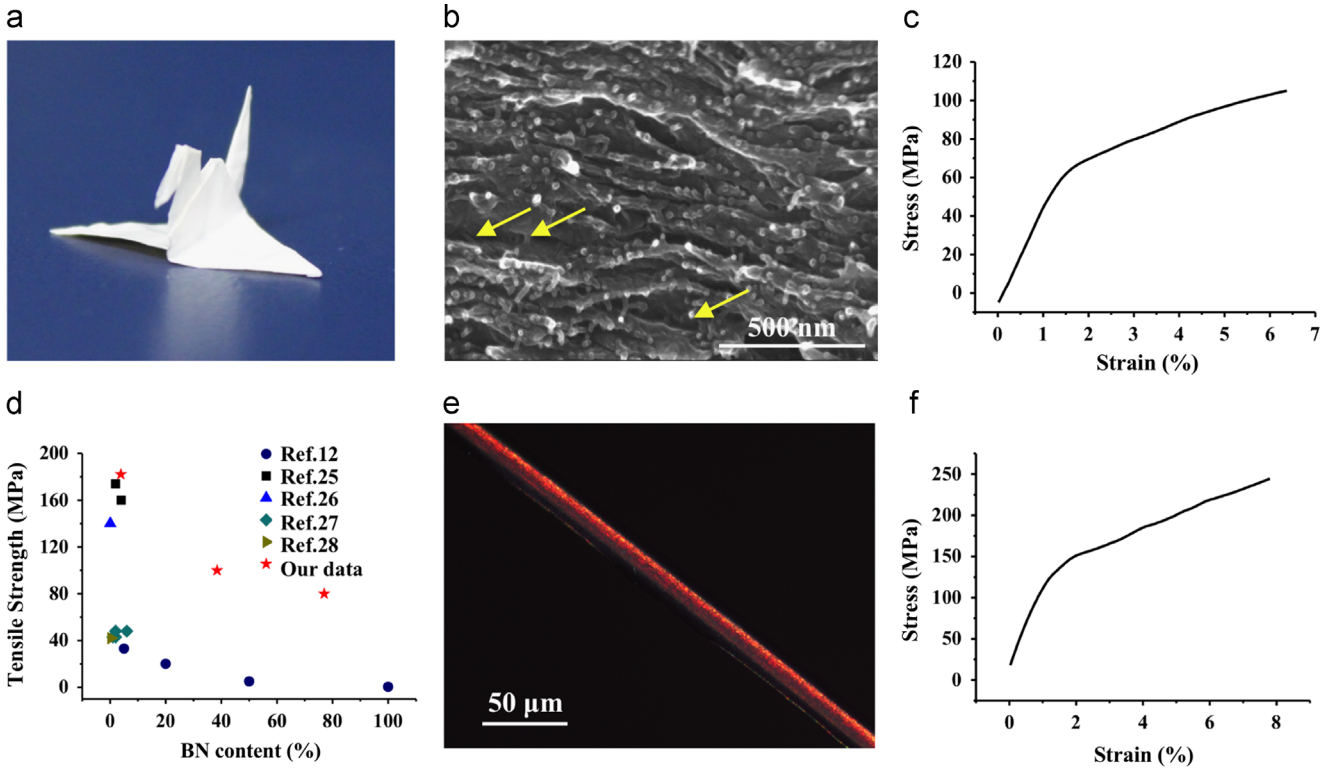

Fig. 5 (a) An origami crane made from the strong, flexible BN film. (b) SEM image showing the cross section of the BN film with a BN flake content of 40 wt%; the arrows refer to NFC. (c) Typical stress-strain curve of the BN composite film with 40 wt% BN. (d) Comparison of the literature for BN composite films where the ultimate tensile strength is plotted against BN content [12,25-28]. (e) A POM image of the BN fiber, demonstrating alignment along the fiber direction. (f) Typical stress-strain curve of the BN fiber with 40 wt% BN.

strong but also flexible enough that knots can be tied with them (Fig. S2d).

For the dispersion of MoS_2, our method allowed for the fabrication of freestanding films with thicknesses ranging from several micrometers to several hundreds of micrometers. A transparent freestanding MoS_2 film with a thickness of 10 μm is shown in Fig. 6a. It is evident by the cross-sectional SEM image (Fig. 6b) that the film is layered, which is advantageous for lithium/sodium ion storage. Fig. S3 is the surface SEM image of the MoS_2 composite film, showing MoS_2 flakes surrounded by NFC. This film possessed a tensile strength of 50±4 MPa. A MoS_2-NFC nanocomposite with even greater tensile strength (159±18 MPa) was obtained when the MoS_2 content decreased to 13 wt% (Fig. 6c). The strength of the film was higher than MoS_2-thermoplastic polyurethane nanocomposites (34 MPa, 5 wt % MoS_2) [12], MoS_2-polyurethane composites (~46 MPa, 15 wt% MoS_2) [34], and MoS_2-polyvinyl alcohol composites (127 MPa, 0.25 wt% MoS_2) [29]. The great mechanical strength was due to the presence of NFC, which was an excellent reinforcing agent and building block to obtain strong films. In addition, the biomimetic nacre structure also contributes to the enhanced mechanical strength.

Multifunctional MoS_2 films can be fabricated in a facile manner by adding functional materials, such as CNTs, to the dispersion. This means that the freestanding MoS_2 films can act as flexible electrodes for lithium or sodium ion battery anodes. To further investigate this, the electrochemical performance of pure MoS_2 paper and MoS_2 composite paper with CNTs as the conductive additive was evaluated against a pure sodium metal counter electrode in a half-cell configuration. The weight ratio of MoS_2:NFC:CNT in the MoS_2 composite paper was 67:16.5:16.5. Note that NFC also dispersed CNTs very well, which allows us to make homogenous MoS_2:NFC:CNT electrode composites. The weight ratio of MoS_2:CNT in pure MoS_2 paper was 83.5:16.5, the same amount of CNT but higher MoS_2 ratio compared with MoS_2 composite paper. The first charge curve of the pure MoS_2 paper battery had a plateau around 0.85 V, which was mainly attributed to the formation of solid electrolyte interface (SEI). The first cycle discharge capacity was 140 mAh/g with a Coulombic efficiency of 37.9%. Fig. 6d shows the MoS_2 composite paper battery charge (sodiation) and discharge (desodiation) curves for the first three cycles in the potential range of 0.1–2.35 V at 10 mA/g. The first charge curve had a similar plateau around 0.85 V, but the first cycle discharge capacity was 147 mAh/g. This value was higher than the pure MoS_2 paper battery anode though with a lower MoS_2 content. This capacity during desodiation even exceeded a MoS_2/Super-P/PEO (60:20:20) composite-based sodium ion battery anode at a current density of 50 mA/g as well as David et al.'s MoS_2/rGO (reduced graphene oxide) composite paper containing 20% MoS_2 at a current density of 25 mA/g. However the performance did not surpass MoS_2/rGO composite paper containing 60% MoS_2 [8,43]. The Coulombic efficiency of the first cycle was 43.8%, better than the pure MoS_2 paper battery. The Coulombic efficiency increased to 89.7% by the third cycle. Overall, these tests demonstrated the feasibility of using NFC dispersed MoS_2 films as sodium ion battery anodes.

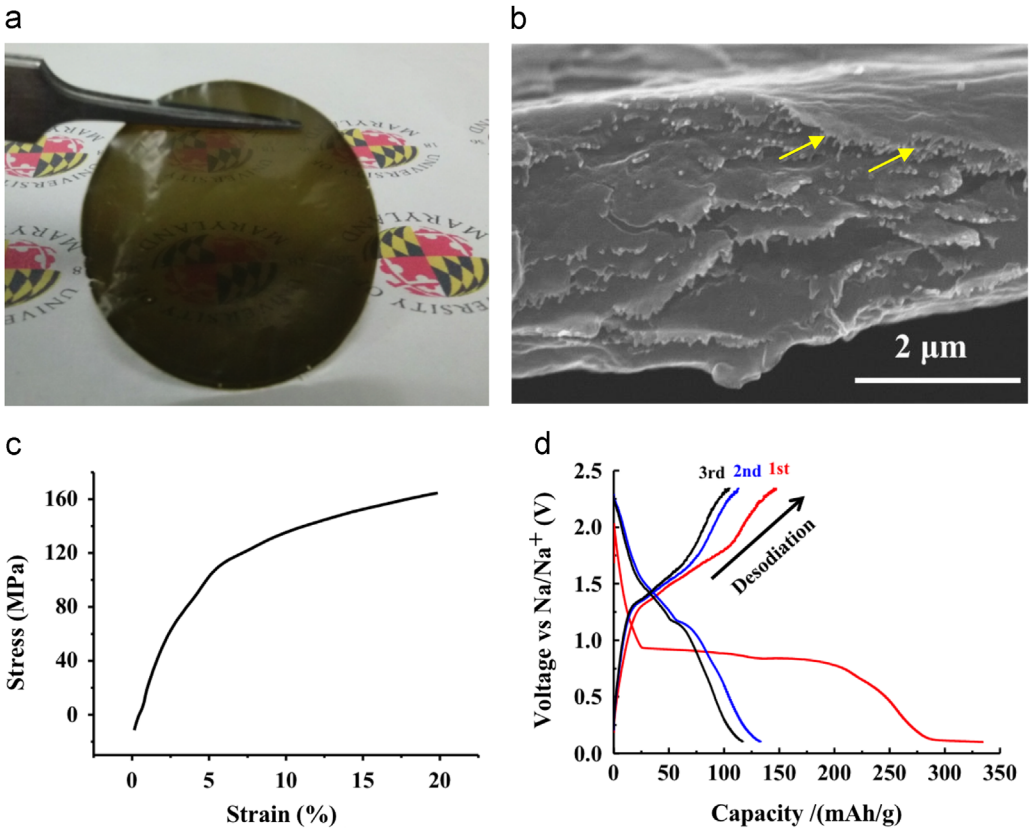

Fig. 6 (a) A digital image of the MoS_2 film. (b) SEM image showing the cross section of the MoS_2 film; the arrows refer to NFC. (c) Typical stress-strain curve of the MoS_2-NFC film with 13 wt% MoS_2. (d) Charge (sodiation) and discharge (desodiation) voltage profiles of the sodium ion battery for the first three cycles at 10 mA/g using an MoS_2 composite film as the working electrode.

Conclusions

We have demonstrated a method to prepare high-quality water-based 2D material dispersions using NFC as a dispersant. This new dispersion method is scalable and environmentally friendly due to the use of a unique green dispersant and the most popular green solvent, water. Multifunctional water-based hybrid solutions can be fabricated in a facile manner by adding other functional materials to the aforementioned solution, enabling potential applications in electronics, energy storage devices as well as in the life sciences. Mechanically strong, functional films and fibers were produced based on the exfoliated BN and MoS_2 solutions. The fabricated MoS_2 films with a layered structure were effectively demonstrated as sodium ion battery anodes for potential flexible battery applications.

Acknowledgment

L. Hu acknowledges the support from the DOD (Air Force Office of Scientific Research) Young Investigator Program (FA95501310143) and the startup support from the University of Maryland, College Park. Y. Li would like to thank the support by the Priority Academic Program Development of Jiangsu Higher Education Institutions (PAPD), the Graduate Student Innovation Program of the Jiangsu Province (CXLX12_0531), and National Natural Science Foundation of China (31470599).

Appendix A. Supplementary Information

Supplementary data associated with this article can be found in the online version at doi:10.1016/j.nanoen.2015.02.015.

References

[1] V. Nicolosi, M. Chhowalla, M.G. Kanatzidis, M.S. Strano, J.N. Coleman, Science 340 (2013) 1226419.
[2] C.B. Zhu, X.K. Mu, P.A. van Aken, Y. Yu, J. Maier (Eds.), Angew. Chem. Int. Ed., 53, 2014, pp. 2152–2156.
[3] S.Z. Butler, S.M. Hollen, L.Y. Cao, Y. Cui, J.A. Gupta, H.R. Gutierrez, T.F. Heinz, S.S. Hong, J.X. Huang, A.F. Ismach, E. Johnston-Halperin, M. Kuno, V.V. Plashnitsa, R.D. Robinson, R.S. Ruoff, S. Salahuddin, J. Shan, L. Shi, M.G. Spencer, M. Terrones, W. Windl, J.E. Goldberger, ACS Nano 7 (2013) 2898–2926.
[4] H.L. Zhu, Y.Y. Li, Z.Q. Fang, J.J. Xu, F.Y. Cao, J.Y. Wan, C. Preston, B. Yang, L.B. Hu, ACS Nano 8 (2014) 3606–3613.
[5] J. Yin, X.M. Li, J.X. Zhou, W.L. Guo, Nano Lett. 13 (2013) 3232–3236.
[6] Y. Lin, J.W. Connell, Nanoscale 4 (2012) 6908–6939.
[7] M.S. Xu, T. Liang, M.M. Shi, H.Z. Chen, Chem. Rev. 113 (2013) 3766–3798.
[8] L. David, R. Bhandavat, G. Singh, ACS Nano 8 (2014) 1759–1770.
[9] L. Liao, J. Zhu, X.J. Bian, L.N. Zhu, M.D. Scanlon, H.H. Girault, B.H. Liu, Adv. Funct. Mater. 23 (2013) 5326–5333.
[10] A. Splendiani, L. Sun, Y.B. Zhang, T.S. Li, J. Kim, C.Y. Chim, G. Galli, F. Wang, Nano Lett. 10 (2010) 1271–1275.
[11] G. Eda, H. Yamaguchi, D. Voiry, T. Fujita, M.W. Chen, M. Chhowalla, Nano Lett. 11 (2011) 5111–5116.
[12] J.N. Coleman, M. Lotya, A. O'Neill, S.D. Bergin, P.J. King, U. Khan, K. Young, A. Gaucher, S. De, R.J. Smith, I.V. Shvets, S.K. Arora, G. Stanton, H.Y. Kim, K. Lee, G.T. Kim, G.S. Duesberg, T. Hallam, J.J. Boland, J.J. Wang, J.F. Donegan, J.C. Grunlan, G. Moriarty, A. Shmeliov, R.J. Nicholls, J.M. Perkins, E.M. Grieveson, K. Theuwissen, D.W. McComb, P.D. Nellist, V. Nicolosi, Science 331 (2011) 568–571.
[13] Z.B. Yang, H. Sun, T. Chen, L.B. Qiu, Y.F. Luo, H.S. Peng, Angew. Chem. Int. Ed. 52 (2013) 7545–7548.
[14] Y.G. Yao, L. Tolentino, Z.Z. Yang, X.J. Song, W. Zhang, Y.S. Chen, C.P. Wong, Adv. Funct. Mater. 23 (2013) 3577–3583.
[15] X. Huang, Z.Y. Zeng, H. Zhang, Chem. Soc. Rev. 42 (2013) 1934–1946.
[16] Y.Y. Li, H.L. Zhu, M. Xu, Z.L. Zhuang, M.D. Xu, H.Q. Dai, BioResources 9 (2014) 1986–1997.
[17] H.L. Zhu, Z.Q. Fang, C. Preston, Y.Y. Li, L.B. Hu, Energy Environ. Sci. 7 (2014) 269–287.
[18] Y.Y. Li, H.L. Zhu, H.B. Gu, H.Q. Dai, Z.Q. Fang, N.J. Weadock, Z.H. Guo, L.B. Hu, J. Mater. Chem. A 1 (2013) 15278–15283.
[19] H.L. Zhu, Z.G. Xiao, D.T. Liu, Y.Y. Li, N.J. Weadock, Z.Q. Fang, J.S. Huang, L.B. Hu, Energy Environ. Sci. 6 (2013) 2105–2111.
[20] C.N. Wu, T. Saito, S. Fujisawa, H. Fukuzumi, A. Isogai, Biomacromolecules 13 (2012) 1927–1932.
[21] I. Siro, D. Plackett, Cellulose 17 (2010) 459–494.
[22] C. Olivier, C. Moreau, P. Bertoncini, H. Bizot, O. Chauvet, B. Cathala, Langmuir 28 (2012) 12463–12471.
[23] M. Andresen, P. Stenius, J. Dispers. Sci. Technol. 28 (2007) 837–844.
[24] M.M. Hamedi, A. Hajian, A.B. Fall, K. Håkansson, M. Salajkova, F. Lundell, L. Wågberg, L.A Berglund, ACS Nano 8 (2014) 2467–2476.
[25] Y. Wang, Z.X. Shi, J. Yin, J. Mater. Chem. 21 (2011) 11371–11377.
[26] U. Khan, P. May, A. O'Neill, A.P. Bell, E. Boussac, A. Martin, J. Semple, J.N. Coleman, Nanoscale 5 (2013) 581–587.
[27] X.B. Wang, A. Pakdel, C.Y. Zhi, K. Watanabe, T. Sekiguchi, D. Golberg, Y. Bando, J. Phys. Condens. Mater. 24 (2012) 314205.
[28] C.Y. Zhi, Y. Bando, C.C. Tang, H. Kuwahara, D. Golberg, Adv. Mater. 21 (2009) 2889–2893.
[29] A. O'Neill, U. Khan, J.N. Coleman, Chem. Mater. 24 (2012) 2414–2421.
[30] Y.Y. Li, H.L. Zhu, F. Shen, J.Y. Wan, X.G. Han, J.Q. Dai, H. Q. Dai, L.B. Hu, Adv. Fuct. Mater. 5 (2014) 7366–7372.
[31] M. Yi, Z.G. Shen, W. Zhang, J.Y. Zhu, L. Liu, S.S. Liang, X.J. Zhang, S.L. Ma, Nanoscale 5 (2013) 10660–10667.
[32] P. May, U. Khan, J.M. Hughes, J.N. Coleman, J. Phys. Chem. C 116 (2012) 11393–11400.
[33] Z.Y. Zeng, Z.Y. Yin, X. Huang, H. Li, Q.Y. He, G. Lu, F. Boey, H. Zhang, Angew. Chem. Int. Ed. 50 (2011) 11093–11097.
[34] R.J. Smith, P.J. King, M. Lotya, C. Wirtz, U. Khan, S. De, A. O'Neill, G.S. Duesberg, J.C. Grunlan, G. Moriarty, J. Chen, J.Z. Wang, A.I. Minett, V. Nicolosi, J.N. Coleman, Adv. Mater. 23 (2011) 3944–3948.
[35] Y. Lin, T.V. Williams, T.B. Xu, W. Cao, H.E. Elsayed-Ali, J.W. Connell, J. Phys. Chem. C 115 (2011) 2679–2685.
[36] Y.C. Wang, J.Z. Ou, S. Balendhran, A.F. Chrimes, M. Mortazavi, D.D. Yao, M.R. Field, K. Latham, V. Bansal, J.R. Friend, S. Zhuiykov, N.V. Medhekar, M.S. Strano, K. Kalantar-zadeh, ACS Nano 7 (2013) 10083–10093.
[37] J.N. Coleman, Acc. Chem. Res. 46 (2013) 14–22.
[38] S. Besombes, K. Mazeau, Plant Physiol. Biochem. 43 (2005) 299–308.
[39] K. Mazeau, Carbohydr. Polym. 84 (2011) 524–532.
[40] X.M. Feng, X. Wang, W.Y. Xing, K.Q. Zhou, L. Song, Y. Hu, Compos. Sci. Technol. 93 (2014) 76–82.
[41] S.Y. Gu, X.F. Gao, Y.H. Zhang, Mater. Chem. Phys. 149–150 (2015) 587–593.

[42] A. Walther, I. Bjurhager, J.M. Malho, J. Pere, J. Ruokolainen, L.A. Berglund, O. Ikkala, Nano Lett. 10 (2010) 2742–2748.
[43] J. Park, J.S. Kim, J.W. Park, T.H. Nam, K.W. Kim, J.H. Ahn, G. Wang, H.J. Ahn, Electrochim. Acta 92 (2013) 427–432.

Yuanyuan Li is a Ph.D. candidate at the College of Light Industry Science and Engineering at Nanjing Forestry University. She is currently an exchange student at the Department of Materials Science and Engineering, University of Maryland. Her research interests include nanomaterials, multifunctional fibers and flexible electronics.

Dr. Hongli Zhu is currently a research associate at the University of Maryland, focusing on the research of environmentally friendly green materials and green energy storage. She received her Ph.D. in Wood and Paper Science from the South China University of Technology, Western Michigan University Alliance in 2009. From 2009 to 2011, Dr. Hongli Zhu conducted research on materials science and processing of biodegradable and renewable biomaterials in the KTH Royal Institute of Technology in Sweden.

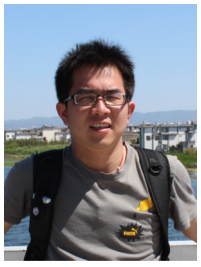

Fei Shen is a Ph.D. candidate of Nanjing University. Currently, he is visiting at the Department of Materials Science and Engineering, University of Maryland, College Park. His research interests include nanomaterials and nanostructures for energy storage and conversion.

Jiayu Wan is a Ph.D. candidate at Department of Materials Science and Engineering, University of Maryland, College Park. His research with Professor Liangbing Hu is on energy storage (Li ion batteries and Na ion batteries, with macro/nano scale studies) and flexible electronics. He received his B. S. degree from Huazhong University of Science and Technology in China in 2011.

Steven Lacey received his B.S. in Materials Science and Engineering (MSE) from the University of Maryland, College Park and is a current Ph.D. candidate in the MSE Department. His current research with Professor Liangbing Hu focuses on the nanomechanics and electrochemical properties of the solid electrolyte interface of two dimensional battery electrodes.

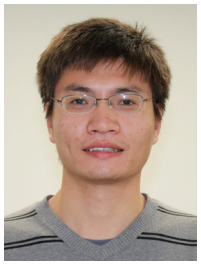

Zhiqiang Fang is a Ph.D. candidate at the State Key Laboratory of Pulp and Paper Engineering for the South China University of Technology, and is currently an exchange student at the Department of Materials Science and Engineering, University of Maryland, College Park. His current research interests include nanomaterials and paper for flexible electronics and energy storage devices.

Hongqi Dai received his B.S. in Pulp and Paper Making Engineering from Nanjing Forestry University (NFU) in 1986 and received his Ph.D. degree in Chemical Processing Engineering of Forest Products from NFU in 2000. Currently, he is a professor at NFU. His research interests include wet end chemistry and its mechanism of paper-making, whitewater closure, cleaner production technology, surface functionalization on paper, development and application of paper chemicals and functional paper.

Liangbing Hu received his B.S. in applied physics from the University of Science and Technology of China (USTC) in 2002. He did his Ph.D. at ***UCLA***, focusing on carbon nanotube based nanoelectronics. In 2006, he joined ***Unidym Inc***. as a co-founding scientist. At Unidym, Liangbing's role was the development of rollto-roll printed carbon nanotube transparent electrodes and device integrations into touch screens, LCDs, flexible OLEDs and solar cells. He worked ***at Stanford University*** from 2009 to 2011, where he work on various energy devices based on nanomaterials and nanostructures. Currently, he is an ***assistant professor at University of Maryland College Park***. His research interests include nanomaterials and nanostructures, roll-to-roll nanomanufacturing, energy storage and conversion, and printed electronics.